Improved Semi-Automatic Basket Catheter Reconstruction from two X-ray Views

Xia Zhong[1], Matthias Hoffmann[1], Norbert Strobel[2], Andreas Maier[1,3]

[1]Pattern Recognition Lab, Friedrich-Alexander-Universität Erlangen-Nürnberg, Erlangen, Germany
[2]Siemens Healthcare GmbH, Forchheim, Germany
[3]Erlangen Graduate School in Advanced Optical Technologies (SAOT)
xia.zhong@fau.de

Abstract. Ablation guided by focal impulse and rotor mapping (FIRM) is an alternative treatment for atrial fibrillation in particular for persistent atrial fibrillation. To this end, a basket catheter comprising 64 electrodes is inserted into both the right atrium and left atrium under X-ray guidance to locate electric anomalies. The 3-D positions of the electrodes are needed to determine the ablation region. We propose a improved model-based method for 3-D reconstruction of this basket catheter based on two X-ray views. In our experiments, we found that the proposed approach outperformed our previous approach. The median error using the proposed method are 1.5 mm for phantom data and 2.6 mm for clinical data. We also introduced a novel error metric, the overlap rate between ground truth ablation region and reconstructed ablation region. The overall mean overlap rate under optimized viewing angle conditions is $84 \pm 14\%$ for phantom data and $72 \pm 16\%$ for clinical data.

1 Introduction

Atrial fibrillation (Afib) is the most common heart rhythm disorder. Ablation guided by focal impulse and rotor mapping (FIRM) has been proposed as a new treatment option. Clinical evaluations performed in the US suggests that FIRM-based ablation offers better long-term outcomes in particular for patients with persistent Afib [1]. A multielectrode basket catheter is used in a FIRM-guided ablation. The basket catheter is placed first in the right atrium and then moved into left atrium during the treatment. The basket catheter has eight splines, each spline comprises eight electrodes. The electrical anomalies and their positions, which are relative to the splines and the electrodes, are found using the Topera Rhythm View 3-D electrophysiological mapping system (Topera Inc., Pal Alto, CA, USA). However, for ablation, a method is required to remap impulse or rotor positions, initially only known relative to the basket, to their associated anatomical positions.

Currently, the EnSite Velocity mapping system (St. Jude Medical, St. Paul, MN, USA) is used to show the ablation region relative to the ablation catheter.

Unfortunately, not only does the use of this mapping system increase the cost of the procedure, it may also introduce inaccuracies due to electrical field distortions [2]. Our previous paper [3] proposed an alternative navigation method using X-ray images to reconstruct the basket catheter relative to the coordinate system of C-arm X-ray imaging system. Good results were found during experiments involving phantoms, but results obtained for clinical data left room for improvement. This is why we present an improved method based on our previous approach. We also combined this with a more in-depth evaluation of the proposed method with respect to clinical data.

1.1 Related Work

Many image based 3-D device detection or reconstruction methods have been proposed already. Hoffman et al. [4] suggested a graph based method to reconstruct catheters from two views. Canero et al. [5] proposed a method using B-snakes to formulate catheter detection as an energy minimization problem. Hasse et al. [6] introduced a 3-D attenuation model based method for ablation catheter detection. Barbu et al. [7] proposed a learning based method to detect guidewires.

In this paper, we suggest an improved version of our previous method [3] to reconstruct a basket catheter from two views. The original method comprises three steps - catheter model training, detection of electrodes and splines, as well as model initialization and adaption. In the first step, a basket catheter spline model is set up. Using this model, the basket catheter can be described as

$$\boldsymbol{M}(\boldsymbol{b}_1, \ldots, \boldsymbol{b}_8, \alpha_1, \ldots, \alpha_8) = \{\boldsymbol{p}_{k,j} | k, j = 1, \ldots, 8\}. \tag{1}$$

where $\boldsymbol{p}_{k,j}$ is the j^{th} electrode on the k^{th} spline. The parameter $\boldsymbol{b}_k$ denotes the shape of the k^{th} spline, and α_k reflects the spline rotation. In the second step, the potential positions of electrodes $\mathcal{E}^{\text{A}}$, $\mathcal{E}^{\text{B}}$ and potential splines $\mathcal{S}^{\text{A}}$, $\mathcal{S}^{\text{B}}$ in image plane A and B are detected. The potential electrode positions make up a 3-D point cloud $\mathcal{E}^{\text{3D}}$. In the third step, multiple basket catheter models are initialized by assuming the deformation parameter $\boldsymbol{b}_k$ is identical for each spline. We refer to this initialization as symmetric initialization. The i^{th} symmetric model in all N initialization models can be described as $\boldsymbol{M}_i(\boldsymbol{b}_i, \ldots, \boldsymbol{b}_i, \alpha_{i,1}, \ldots, \alpha_{i,8})$. Each model $\boldsymbol{M}_i$ must satisfy the length constraint. The overall length of the basket catheter is obtained by having the user select start point, end point, and at least one of eight marker electrodes in both views. The rotation of the model can then be estimated using the 3-D point cloud and 2-D features found in the X-ray images. When using 2-D features, rotation estimation can be formulated as an

optimization problem by introducing the energy term $\mathcal{D}$ as follows

$$\begin{aligned}\mathcal{D}(\boldsymbol{b},\boldsymbol{\alpha}) = a_1 \cdot \underbrace{(\textstyle\sum_i \min_k d(\boldsymbol{e}_i^{\mathrm{A}}, \boldsymbol{S}_k^{\mathrm{A}}(\boldsymbol{b}_k,\alpha_k)) + \sum_i \min_k d(\boldsymbol{e}_i^{\mathrm{B}}, \boldsymbol{S}_k^{\mathrm{B}}(\boldsymbol{b}_k,\alpha_k)))}_{\text{Distance of each detected electrode to projected splines of the model}} \\ a_2 \cdot \underbrace{(\textstyle\sum_i \min_{j,k} d(\boldsymbol{e}_i^{\mathrm{A}}, \boldsymbol{p}_{k,j}^{\mathrm{A}}(\boldsymbol{b}_k,\alpha_k)) + \sum_i \min_{j,k} d(\boldsymbol{e}_i^{\mathrm{B}}, \boldsymbol{p}_{k,j}^{\mathrm{B}}(\boldsymbol{b}_k,\alpha_k)))}_{\text{Distance of each detected electrode to projected electrodes of the model}} \\ a_3 \cdot \underbrace{(\textstyle\sum_{k,j} \min_i d(\boldsymbol{e}_i^{\mathrm{A}}, \boldsymbol{p}_{k,j}^{\mathrm{A}}(\boldsymbol{b}_k,\alpha_k)) + \sum_{k,j} \min_i d(\boldsymbol{e}_i^{\mathrm{B}}, \boldsymbol{p}_{k,j}^{\mathrm{B}}(\boldsymbol{b}_k,\alpha_k)))}_{\text{Distance of each projected electrode of the model to detected electrodes}}\end{aligned} \tag{2}$$

The rotation $\boldsymbol{\alpha}_i$ of model $\boldsymbol{M}_i$ is estimated by minimizing $\mathcal{D}$. Then, the model $\boldsymbol{M}_{\min}$ which corresponds to lowest value of $\mathcal{D}$ will be used as the model for image based model adaption. A regularization term $\mathcal{R}$ is introduced here to perform a combined optimization when calculating deformation and rotation

$$\boldsymbol{b},\boldsymbol{\alpha} = \underset{\boldsymbol{b}_1 \ldots \boldsymbol{b}_8, \alpha_1, \ldots, \alpha_8}{\operatorname{argmin}} \mathcal{D}(\boldsymbol{b}_1,\ldots,\boldsymbol{b}_8,\alpha_1,\ldots,\alpha_8) + \mathcal{R}(\boldsymbol{b}_1,\ldots,\boldsymbol{b}_8,\alpha_1,\ldots,\alpha_8) \tag{3}$$

2 Materials and Methods

While using a similar approach as stated in previous paper, we made modifications to the second and the third step to improve the outcomes. First, a more robust electrode detection algorithm was implemented to reduce the false positive rate. False detection is mainly caused by the presence of other catheters and devices during the intervention. Given the fact that electrodes of the basket catheter are different in size and attenuation from other instruments, we applied suitably selected threshold to our detection results to distinguish basket catheter electrodes from other objects. Second, the assumption of a symmetric basket catheter model in the initialization step was relaxed. Instead, we propose to construct an asymmetric basket catheter which is closer to the clinical environment and search for the best asymmetric basket catheter model during our optimization step.

2.1 Electrode Detection

We first use the same method in our former paper to extract the positions of electrode candidates $\mathcal{E}^{\mathrm{A}}$ and $\mathcal{E}^{\mathrm{B}}$ in both image planes based on the estimated pixel size w_{im} in the X-ray image. We defined a neighborhood $\mathcal{W}_i^{\mathrm{A}}$ for the i^{th} electrode candidate $\boldsymbol{e}_i^{\mathrm{A}}$ in image A with a size of $4w_{\mathrm{im}} \times 4w_{\mathrm{im}}$. Respectively $\mathcal{W}_i^{\mathrm{B}}$ denotes the neighborhood for $\boldsymbol{e}_i^{\mathrm{B}}$. We then perform an unsharp masking for each $\mathcal{W}_i^{\mathrm{A}}$ followed by binarization using Otsu thresholding. In the binary image we then calculate the areas of pixels connected to the electrode candidates. We trained a threshold to classify whether the electrodes belong to the basket catheter.

2.2 Asymmetric Model Initialization

In last paper, we assumed symmetric basket catheter models in the initialization step. The model which showed the best fit according to the energy term $\mathcal{D}$ was chosen for image based adaption. We refined this step by allowing the model to be asymmetric. Let $\boldsymbol{M}_i(\boldsymbol{b}_i, \ldots, \boldsymbol{b}_i, \alpha_{i,1}, \ldots, \alpha_{i,8})$ be the i^{th} symmetric model of N models sorted in ascending order of corresponding $\mathcal{D}$ value. We now construct an asymmetric model as a combination of these N models and arrive at $\boldsymbol{M}^{\text{ASY}}(\boldsymbol{b}_1^{\text{ASY}}, \ldots, \boldsymbol{b}_8^{\text{ASY}}, \boldsymbol{\alpha}^{\text{ASY}})$ where $\boldsymbol{b}_n^{\text{ASY}} \in \{\boldsymbol{b}_i | i = 1, \ldots, N\}$, $\boldsymbol{\alpha}^{\text{ASY}} \in \{\alpha_{i,j} | i = 1, \ldots, N; j = 1, \ldots, 8\}$. When $\boldsymbol{b}_n^{\text{ASY}} = \boldsymbol{b}_i$, we assume $\alpha_n^{\text{ASY}} = \alpha_{i,n}$ for simplicity. The problem of finding the best asymmetric model can be addressed by solving the following combinatorial optimization problem.

$$\{\boldsymbol{b}_n^{\text{ASY}} | n = 1, \ldots, 8\} = \underset{\{\boldsymbol{b}_n | n=1,\ldots,8\} \in \boldsymbol{b}_i}{\operatorname{argmin}} \mathcal{D}(\boldsymbol{b}_1^{\text{ASY}}, \ldots, \boldsymbol{b}_8^{\text{ASY}}, \boldsymbol{\alpha}^{\text{ASY}}) \tag{4}$$

The computational complexity to perform a full search is $\mathcal{O}(N^8)$. We reduced the complexity by choosing the first $m < N$ of the weighting factors $\{\boldsymbol{b}_i | i = 1, \ldots, N\}$ and optimize Eq. 4 by greedy search. The complexity is reduced to $\mathcal{O}(mt)$ where t denotes the number iterations for greedy search.

2.3 Evaluation

We carried out two different evaluations. First, we compared our new approach to previous method based on available phantom data and clinical data. In all, 18 sets of phantom data and 8 sets of clinical data were evaluated. The basket catheter in phantom data has an identical radius of 60 mm while in clinical data the radius of the basket catheter varies between 50, 60, and 70 mm depending on the patient. We evaluated the distance between the reconstructed basket catheter electrodes and ground truth electrodes. Second, we introduced an ablation region overlap rate evaluation which we find more clinically relevant. In a FIRM-guided ablation procedure, the ablation region is usually defined by neighboring electrodes on neighboring splines around a rotor region [1]. The evaluation is to calculate the overlap between the ablation region region defined by four electrodes either derived from ground truth and reconstructed model. We express this overlap as a overlap rate defined as the area of intersection between estimated and ground truth ablation region divided by area of the ground truth ablation region.

3 Results

We first show the results of a comparison using the original method and the proposed method in Fig. 1. The results of our comparison between the original an the proposed algorithm are shown in Fig. 2. The graphs show that the proposed method outperforms the original approach. Median errors on phantom data using the former method were 1.7 mm using a single marker electrode for initialization and 1.6 mm when involving all eight marker electrodes, respectively. Using the

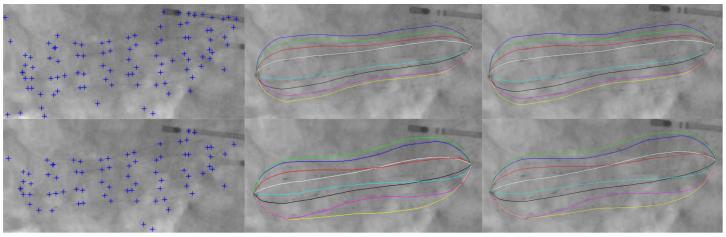

Fig. 1. Result in electrodes detection (left), model initialization (middle), and model adaption using original method (first row) and proposed method (second row) on the same X-ray images. The blue crosses denotes the detected position of electrode candidates. As shown in the figure, the previous method also detects electrodes of ablation catheter (upper right in each images) while proposed method reduce the number of detection error.

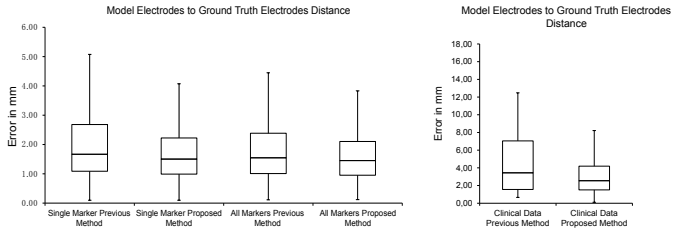

Fig. 2. Evaluation using previous method vs. proposed method in phantom data (left) and clinical data (right). Single marker refers to initialization using one marker electrode, and all markers refers to initialization using each marker electrode on every spline.

new method, the error reduced to 1.5 mm for both cases. When evaluating clinical data, the median error improved from 3.4 mm with the original approach to 2.6 mm for the proposed method using a single marker. Applying the proposed method, the median errors in the phantom data and the clinical data are below the clinical important threshold of 3 mm [8]. The results of the overlap rate evaluation are shown in Fig. 3. Using the initial C-arm view angles, the mean overlap rate is $67 \pm 29\%$ for the phantom data and $56 \pm 28\%$ for the clinical data. The viewing angle can be optimized by aligning the view angle with the normal vector according to the estimated patch of interest. If we assume such a view configuration, the overall mean overlap rate is $84 \pm 14\%$ for the phantom data and $72 \pm 16\%$ for the clinical data respectively.

4 Discussion

Our results demonstrate that the proposed approach outperforms our previous method especially for clinical data. By applying a more robust electrode detection, fewer false electrodes were used to estimate the basket catheter model. The

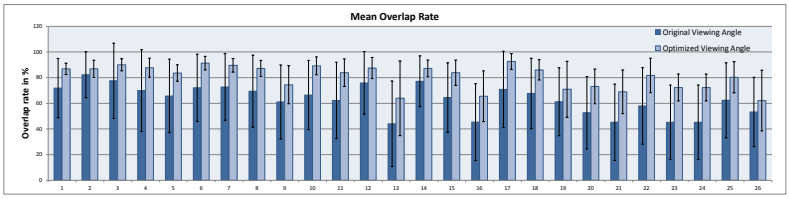

Fig. 3. Mean overlap rate between estimated ablation region and ground truth ablation region in phantom data (1-18) and clinical data (19-26)

asymmetric model allowed a more realistic initialization. The initialization is very important for successful 2D/3D registration due to the high number of local minima in high dimensional optimization space. The overlap rate evaluation reveals that the overlap rate largely depends on the viewing angle. Adjusting viewing angles properly, we could increase the mean overlap rate by 15%, and this way provide a better view on the ablation region.

Acknowledgments We gratefully acknowledge the feedback given to us by the Klinikum Coburg, Germany, and we would also like to thank them for the test images. This work was supported by Siemens Healthcare GmbH, Forchheim, Germany. The concepts and information presented in this paper are based on research, and are not commercially available.

References

1. Narayan SM, Krummen DE, Shivkumar K, et al. Treatment of Atrial Fibrillation by the Ablation of Localized Sources: {CONFIRM} Trial. J Am Coll Cardiol. 2012;60(7):628–636.
2. Eitel C, Hindricks G, Dagres N, et al. EnSite Velocity cardiac mapping system: a new platform for 3D mapping of cardiac arrhythmias. Expert Rev Med Devices. 2010;7(2):185–192.
3. Zhong X, Hoffmann M, Strobel N, Maier A. Semi-Automatic Basket Catheter Reconstruction from Two X-Ray Views. Proc GCPR. 2015;9358:379–389.
4. Hoffmann M, Brost A, Koch M, et al. Electrophysiology Catheter Detection and Reconstruction from Two Views in Fluoroscopic Images. IEEE Trans Med Imaging. 2015 ahead of print;.
5. Canero C, Radeva P, Toledo R, et al. 3D curve reconstruction by biplane snakes. Proc Pattern Recognit. 2000;4:563–566.
6. Haase C, Schaefer D, Doessel O, Grass M. 3D ablation catheter localisation using individual C-arm x-ray projections. Phys Med Biol. 2014;59(22):6959.
7. Barbu A, Athitsos V, Georgescu B, et al. Hierarchical Learning of Curves Application to Guidewire Localization in Fluoroscopy. Proc IEEE Comput Soc Conf Comput Vis Pattern Recognit. 2007; p. 1–8.
8. Bourier F, Fahrig R, Wang P, et al. Accuracy Assessment of Catheter Guidance Technology in Electrophysiology Procedures. J Cardiovasc Electrophysiol. 2014;25(1):74–83.